



LAWRENCE
LIVERMORE
NATIONAL
LABORATORY

Statistical line-by-line model for atomic spectra in intermediate coupling

C. Iglesias

February 21, 2012

High energy density physics

Disclaimer

This document was prepared as an account of work sponsored by an agency of the United States government. Neither the United States government nor Lawrence Livermore National Security, LLC, nor any of their employees makes any warranty, expressed or implied, or assumes any legal liability or responsibility for the accuracy, completeness, or usefulness of any information, apparatus, product, or process disclosed, or represents that its use would not infringe privately owned rights. Reference herein to any specific commercial product, process, or service by trade name, trademark, manufacturer, or otherwise does not necessarily constitute or imply its endorsement, recommendation, or favoring by the United States government or Lawrence Livermore National Security, LLC. The views and opinions of authors expressed herein do not necessarily state or reflect those of the United States government or Lawrence Livermore National Security, LLC, and shall not be used for advertising or product endorsement purposes.

Statistical line-by-line model for atomic spectra in intermediate coupling

CARLOS A. IGLESIAS
Lawrence Livermore National Laboratories
P.O. Box 808, Livermore, CA 94550, USA

Abstract

The partially resolved transition array (PRTA) model is extended from JJ to intermediate coupling. The PRTA model conserves known array properties, yields improved higher moments, and systematically accounts for initial level populations. In addition, a random PRTA (R-PRTA) model is proposed to simulate detailed line accounting (DLA) calculations of complex spectra. Numerical examples show that the PRTA model with intermediate coupling reproduces the effects of the electrostatic interaction between spin-orbit split arrays on the spectrum. They also show that the R-PRTA model is in good agreement with DLA results and accounts for systematic line coincidences across transition arrays differing only in the subshell occupation of excited spectator electrons important in opacity calculations. Both PRTA and R-PRTA models are computationally much faster than DLA calculations. Hence, the models can accelerate spectrum calculations without introducing significant uncertainties whenever the DLA method is considered arduous or impractical.

Keywords:

Plasma spectroscopy, transition arrays, opacity, emissivity

Corresponding author:

e-mail: iglesias1@llnl.gov (C. A. Iglesias)

1. Introduction

An accurate description of plasma radiative properties is important in many research areas such as astrophysics and inertial confinement. For plasmas containing partially ionized atoms the detailed line accounting (DLA) method is, in principle, the ideal approach to calculate bound-bound spectra. For complex ions, however, the myriad spectral lines make DLA calculations impractical [1]. One approach to circumvent this impasse is the unresolved transition array (UTA) model where the lines are treated as a single unresolved feature [2,3]. The UTA model gives compact formulas for the transition array strength-weighted energy mean and variance that together with a Gaussian assumption for the line energy-strength correlation function allows for a fast calculation of the spectrum.

The UTA approach, however, introduces uncertainties due to inaccurate higher moments [4,5]. Furthermore, conditions exist where the array lines do not merge and the “porosity” of the spectrum makes the plasma more transparent to radiation than predicted by the UTA model. For example, in stellar envelopes the low matter density leads to narrow spectral lines and Rosseland mean opacity calculations with the UTA approach significantly overestimate DLA results [6].

Transition arrays requiring intermediate coupling are also challenging for UTA approaches and there is no exact statistical formalism that progressively describes the transition of the single feature in the near-LS case towards the spin-orbit split relativistic sub-arrays. Models have been developed to account for this effect [7,8], but these require approximations.

Recently an extension of the UTA approach to complement DLA calculations in JJ coupling was developed [9]. The partially resolved transition array (PRTA) model replaces the single feature of the UTA by a number of Gaussians that conserve the known arrays properties, provides improved higher moments, and accounts for initial level populations.

The present work has two main goals. The first is to extend the PRTA model to intermediate coupling. The second is to propose a statistical simulation of DLA results based on the PRTA method. Section 2 briefly reviews the PRTA method and presents the modifications for intermediate coupling. Section 3 describes a statistical approach to simulate DLA calculations using the PRTA model. Numerical examples in both Sections compare results from the PRTA based models to DLA and UTA calculations. The opacity of Fe in stellar envelope conditions is featured in Section 4 comparing results using various approximations for the bound-bound spectrum. Conclusions are offered in the final Section 5.

2. Partially resolved transition array (PRTA) model

Consider a transition array consisting of N spectral lines linking two electronic configurations by a dipole radiative transition. Assuming there are M open subshells in the transition array, then it can be symbolically written as

$$\eta_1^{\alpha_1} \eta_2^{\alpha_2} \lambda_3^{\alpha_3} \dots \lambda_M^{\alpha_M} \rightarrow \eta_1^{\alpha_1-1} \eta_2^{\alpha_2+1} \lambda_3^{\alpha_3} \dots \lambda_M^{\alpha_M} \quad (2.1)$$

where η and λ denote subshell quantum numbers ($n\ell$ or $n\ell j$) and α is the number of electrons occupying the subshell. Here the η 's represent *active* subshells in the transition while the λ 's represent *spectator* or *passive* subshells. The variance of the transition array in Eq. (2.1), assuming the Slater integrals are the same in both configurations, can be written in the form [2,3]

$$\sigma_{tot}^2 = \sigma^2(\eta_1^{\alpha_1} \eta_2^{\alpha_2} \rightarrow \eta_1^{\alpha_1-1} \eta_2^{\alpha_2+1}) + \sum_{m=3}^M \alpha_m (\Pi_m - \alpha_m) \sigma^2(\lambda_m \eta_1 \rightarrow \lambda_m \eta_2) \quad (2.2)$$

where Π_m is the degeneracy of the λ_m subshell.

The PRTA method computes the contribution to the line spectrum by splitting the open subshells into two groups: *main* and *secondary* [9]. An explicit DLA calculation of the main group that is by design small compared to the full DLA calculation is performed. This small-scale DLA calculation generates $K \ll N$ lines by artificially assuming that the subshells in the secondary group are closed, but retains the radial integrals from the self-consistent calculation for the complete configuration. A statistical approach for the secondary group assigns the missing variance in the small-scale DLA calculation to each of the K lines.

In local thermal equilibrium (assumed throughout the work), the PRTA spectrum for the transition array is described by a sum of Gaussians [9],

$$\frac{1}{\sigma_K \sqrt{2\pi}} \sum_{i=1}^K f_i \exp\left\{-\frac{h^2(v - v_i)^2}{2\sigma_K^2}\right\} g_i e^{-\varepsilon_i/T} \quad (2.3)$$

where T is the plasma temperature in energy units. The small-scale DLA calculation for the main group yields f_i and $h\nu_i$ for the oscillator strength and line energy while ε_i and g_i are the energy and degeneracy of the initial level for the i^{th} line. The variance σ_K^2 , assuming the first M_k subshells in Eq. (2.1) define the main group, is given by

$$\sigma_K^2 = \sum_{m=M_k+1}^M \alpha_m (\Pi_m - \alpha_m) \sigma^2(\lambda_m \eta_1 \rightarrow \lambda_m \eta_2) \quad (2.4)$$

and contains the remainder of σ_{tot}^2 from the secondary group not accounted by the K lines.

The PRTA model selects the main and secondary group to balance between accuracy and computational speed. The idea is to include in the main group the subshells that most strongly couple with the active electrons treating the remaining subshells statistically. Although presently this separation is intuitive and not rigorous, it is reasonable to assume those subshells with the largest contribution to the variance couple most strongly with the active electrons [9].

The PRTA model approximately conserves the transition array total oscillator strength, which depends only on the active subshells except for how the spectator electrons affect line energies [10] and exactly conserves the strength-weighted energy mean and variance. The expression in Eq. (2.3) includes Boltzmann factors, which approximate the spectrum dependence on initial level populations. Finally, the Gaussians are convolved with the intrinsic line profile to generate the line spectrum

2.1 RPTA model in intermediate coupling

The form for the variance in Eq. (2.1) is valid in intermediate coupling, but it is complicated by the electrostatic interaction between the relativistic sub-arrays [7,8]. That is, the sub-arrays can overlap or not depending on the relative size of the spin-orbit interaction.

It is convenient to use the LS representation and explicitly separate the spin-orbit interaction contribution to the variance [2],

$$\sigma_{tot}^2 = \sigma_{LS}^2 + \sigma_{SO}^2(\eta_1, \eta_2) \quad (2.1.1)$$

Here σ_{SO}^2 only involves the orbital quantum numbers and spin-orbit radial integrals for the active subshells [11] and

$$\sigma_{LS}^2 = \Omega_{LS}^2(\eta_1^{\alpha_1} \eta_2^{\alpha_2} \rightarrow \eta_1^{\alpha_1-1} \eta_2^{\alpha_2+1}) + \sum_{m=3}^M \alpha_m (\Pi_m - \alpha_m) \Omega_{LS}^2(\lambda_m \eta_1 \rightarrow \lambda_m \eta_2) \quad (2.1.2)$$

with Ω_{LS}^2 the electrostatic interaction contribution for the open subshells. Since the main group always includes the active subshells, the secondary group contribution to the variance is given by

$$\sigma_K^2 = \sum_{m=M_k+1}^M \alpha_m (\Pi_m - \alpha_m) \Omega_{LS}^2(\lambda_m \eta_1 \rightarrow \lambda_m \eta_2). \quad (2.1.3)$$

The selection of the first M_k subshells in Eq. (2.1) for the main group uses

$$R \equiv 1 - (\sigma_K^2 / \sigma_{LS}^2) \quad (2.1.4)$$

rather than comparing σ_k^2 to the total array variance [9]. This reflects that spin-orbit splitting contributes to the total array variance, but not to the individual relativistic sub-array variance [3]. The value $R \geq 0.7$ yielded good results for calculations with JJ coupling [9].

2.2 Calculation details

In the examples below the radial integrals are computed with a Dirac-Hartree-Slater self-consistent field including Breit and QED corrections [12,13] assuming the single configuration approximation. The DLA calculations use intermediate coupling in the LS representation [10], which does not require configuration interaction, so an averaging procedure of the relativistic results is applied [14].

A Voigt profile describes the intrinsic line shape where the Gaussian and Lorentz components are attributed to Doppler and a small natural width Γ , respectively. The small line width minimizes merging of the lines and allows for “porous” line spectra.

The spectrum has temperature dependence from Doppler broadening and Boltzmann weighting of the initial levels. The temperature is chosen so that the ion charge state featured in the example agrees with the ionization average from a Thomas-Fermi [15] calculation at one-hundredth normal density of the material. Thus, the examples are representative of conditions relevant to experiments or laboratory applications.

The fraction of the total variance squared retained in the main group of the PRTA scheme, R in Eq. (2.1.4), is reported in Tables 1 and 2. Also reported in these tables is an estimate of the computational speedup of the PRTA model relative to the full DLA calculation,

$$speedup = t_{DLA} / t_{PRTA} \quad (2.2.1)$$

where t_{DLA} and t_{PRTA} are the times to compute line strengths and positions in the full and small-scale DLA calculations. It is stressed that the speedup does not reflect any timesaving associated with generating the spectrum using a reduced number of lines. This potential savings was excluded since it depends on the number of points in the photon frequency mesh.

2.3 Numerical examples: $3p \rightarrow 3d$ transitions

The PRTA scheme with intermediate coupling is compared with DLA and UTA calculations. The numerical examples in this subsection are the transition $3p \rightarrow 3d$ in the ions Fe^{4+} , In^{27+} , Ba^{34+} , and Tm^{+47} for the initial configuration

$$[Mg]3p^5 3d^3 4s4p \quad (2.3.1)$$

The spectra calculations using DLA and PRTA with the active subshells in the main group are plotted in Figs. 1 through 4 and Table 1 summarizes the results including the number of open subshells and lines in the DLA calculations.

In addition, Figs. 1 through 4 display UTA calculations using the LS basis including the spin-orbit interaction [2] as well as calculations with the spin-orbit split-array method [3] (here referred to as UTA-LS and SOSA, respectively). The figures show the PRTA in better agreement with DLA than either UTA approaches. Most importantly, the PRTA scheme reproduces the transition from near-LS to spin-orbit split arrays. This good agreement applies to the relative strength of the relativistic sub-arrays whereas in Fig. 4 the SOSA model [3] yields good energies and variances for Tm^{+47} compared to the DLA results, but incorrect strength ratio of the relativistic sub-arrays (known limitation of SOSA approach [7,8]). In these examples the PRTA offers about 3 orders of magnitude savings in computational effort compared to the full DLA calculation (see Table 1).

2.4 Numerical examples: $2s \rightarrow 3p$ transitions

The numerical examples in this subsection are for the transition $2s \rightarrow 3p$ in the ions Fe^{5+} , In^{28+} , and Ba^{35+} for the initial configuration

$$[\text{Mg}]3p^4 3d^3 4s4d \quad (2.4.1)$$

Calculations using DLA and PRTA with 3 subshells ($2s3p3d$) in the main group are displayed in Figs. 5 through 7. In these examples the charge states are only modified by one bound electron so the temperature is kept the same as in the previous examples. The Lorentz widths, however, are a factor of 10 larger. Again, the figures show the PRTA in better agreement with DLA than either UTA approaches. In fact, the agreement in Figs. 6 and 7 makes it difficult to differentiate the two calculations. The PRTA model offers more than 3 orders of magnitude savings in computational effort compared to the full DLA calculation (see Table 2).

3. Random partially resolved transition array (R-PRTA)

Figures 1 through 7 show the PRTA model reasonably reproducing the envelope of the DLA results, but not the porosity of the spectrum in the case of non-overlapping lines. Past attempts to simulate DLA results by randomly generating lines relied on approximate energy-strength correlation functions [8,16,17]. The latest model [8] favorably compared with opacity

calculations using full DLA models. The two earlier models [16,17], however, produced significant opacity overestimates for astrophysical plasmas [6].

A partial explanation for the overestimate is that random line generation methods do not retain the near line coincidences of transition arrays having similar configurations with only different excited subshell occupations common in opacity calculations. As an example, Fig. 8 presents spectra for the transition $3p \rightarrow 3d$ for In^{27+} for initial configurations

$$[\text{Mg}]3p^5 3d^3 4snp \quad (3.1)$$

with $n = 4, 5, \text{ and } 6$. These are DLA calculations in intermediate coupling that show a strong correlation of line energies and strengths across transition arrays. The more excited configurations display a small red shift produced by the self-consistent field calculations for the configuration-average energy. There is also a slight narrowing of the features since the more excited spectator electron couples less with the active subshells. Clearly, a random line-by-line simulation of the lines based only on an approximate line envelope can destroy this correlation and fill spectral windows overestimating the opacity.

For comparison Fig. 8 displays PRTA calculations in intermediate coupling (only active subshells in the main group) for the same transitions, but setting $\sigma_K = 0$ in Eq. (2.3). It is stressed that the lines from this calculation are not a subset of the full DLA calculations; that is, the coupling with the secondary group would further split the K lines generated by the main group. There are over a factor of 100 fewer lines compared to the DLA spectrum (see Table 1) and since the PRTA model essentially conserves the total oscillator strength the individual lines are on average much stronger. Consequently, to preserve the scale in Fig. 8, the Lorentz width in the PRTA ($\sigma_K = 0$) calculation was arbitrarily increased by a factor of 10. The figures show that the PRTA ($\sigma_K = 0$) results mimic the line energy-strength behavior of the full DLA calculations. Incidentally, this last comparison helps explain the reasonable success of the PRTA model in reproducing the line envelope from the DLA results in Figs. 1 through 7.

3.1 Random partially resolved transition array (R-PRTA) model

Although it is possible to generate the lines using the envelope in Eq. (2.3), as mentioned above this procedure tends to destroy the correlations across arrays. Instead, it is preferable to simulate the splitting of the K lines from the main group by the electrons in the secondary group. The specific details require a full DLA calculation so it is approximated by splitting the i^{th} line

into n_i lines with random energy and strength based on a Gaussian distribution of variance σ_i . The different n_i and σ_i values for each of the K lines reflect the different coupling between the electrons in the secondary group and the total angular momentum levels generated by the DLA component of the PRTA scheme.

After selecting the main and secondary subshell groups in the transition array as before, the following ansatz relies on two general properties of transition arrays to generate the set $\{n_i, \sigma_i\}$ and bound-bound spectrum:

(1) The number of lines in a transition array is proportional to the product of the number states in the initial and final configurations [18]. Hence, take

$$n_i = N_{est} \times \text{Nearest integer} \left[\frac{(2J_i + 1)(2J'_i + 1)}{\sum_{i=1}^K (2J_i + 1)(2J'_i + 1)} \right] \quad (3.1.1)$$

where J_i and J'_i are the total angular momentum of the initial and final levels of the i^{th} line from the small-scale DLA calculation and N_{est} is the estimated number of total lines in the transition array [18]. The normalization factor in Eq. (3.1.1) cancels the contribution to the number of states from the secondary group common to all K lines and yields

$$\sum_{i=1}^K n_i \approx N_{est} \quad (3.1.2)$$

conserving (within the accuracy of the estimate) the total number of lines in the transition array.

(2) The relatively few strong lines of a transition array are described by a small variance while the much larger number of weak lines are described by a large variance [19]. Thus, σ_i^2 is assumed to have the form

$$\begin{aligned} \sigma_i^2 &\propto \left(\frac{n_i}{s_i} \right) \sigma_K^2 \\ &= \left(\frac{S_K}{N_K} \right) \left(\frac{n_i}{s_i} \right) \sigma_K^2 \end{aligned} \quad (3.1.3)$$

where the total strength of the K lines is given by

$$S_K = \sum_{i=1}^K s_i \quad (3.1.4)$$

with s_i the strength of the i^{th} line and the proportionality constant is constrained by conserving the total transition array variance (see *Appendix*).

(3) Each of the randomly generated n_i lines is dressed with the assumed intrinsic line profile and weighted by the Boltzmann factor for the level population. Specifically, the bound-bound spectrum is proportional to

$$\sum_{i=1}^K g_i e^{-\epsilon_i/T} \sum_{j=1}^{n_i} f_j^{(i)} \phi(\nu - \nu_j^{(i)}) \quad (3.1.5)$$

where $\phi(\nu)$ is the intrinsic line profile with $f_j^{(i)}$ and $\nu_j^{(i)}$ the j^{th} randomly generated line energy and oscillator strength from the i^{th} line from the main group. In addition, the randomly generated position and strength of the n_i lines are adjusted to conserve the strength as well as the strength-weighted energy mean and variance, s_i , $h\nu_i$, and σ_i .

3.2 Numerical details

The proposed random line-by-line (R-PRTA) method entails a slightly larger computational effort than the PRTA scheme. The additional cost involves generating random line energies and strengths from a Gaussian distribution (used Box-Mueller method [20]). For very weak lines ($s_i \leq 10^{-11} S_K$) there can be numerical difficulties associated with a very large variance. Since such lines make insignificant contributions to the spectrum, they are neglected.

Generating the spectrum from myriad lines can present a computational challenge. Here, the spectrum calculation takes advantage of an efficient algorithm based on fast Fourier transform (FFT) techniques [21]. The implementation of this algorithm requires that all N_{est} lines in the transition array have identical profiles so the Doppler width for all the lines assumes the mean transition energy.

3.3 Numerical examples: Excited spectator electrons

The R-PRTA model described in Section 3.1 is applied to the examples with varying spectator subshell and the results displayed in Fig. 8. The comparison of the DLA and R-PRTA calculations in the figure shows good agreement except that in the former the strongest lines are stronger. Most importantly, the R-PRTA method retains the line position and strength correlations across transition arrays.

It is interesting to note that the description of excited spectator electron effects on the intrinsic line profile involves quantum interference phenomena [22]. Furthermore, opacity

calculations can be sensitive to line shape models [23]. These topics, however, are beyond the scope of the present discussion. Since the examples are only intended to evaluate the R-PRTA method, the individual lines in the DLA and R-PRTA calculations in Figs. 8 have identical intrinsic line profiles independent of the spectator electron excitation.

3.4 Numerical examples: $3p \rightarrow 3d$ transition

The R-PRTA model is now applied to the remaining $3p \rightarrow 3d$ examples in Section 2.3. The results are compared in Figs. 9 through 11 (results for In^{27+} are in Fig. 8) showing good agreement with the DLA spectra. As mentioned before, the R-PRTA method does not produce strong enough lines compared to the DLA method. Another shortcoming is the absence of strong features in the shoulder of the transition array. Although these strong lines are present in the DLA calculation of the main group and produce a local maximum, the adopted procedure overestimates their splitting.

3.5 The PRTA model with variable variance

An alternative model for generating the envelope of the transition array using the variable variance procedure in Section 3.1 is possible. The PRTA spectrum with variable variance for the transition array is given by

$$\sum_{i=1}^K \frac{f_i}{\sigma_i \sqrt{2\pi}} \exp\left\{-\frac{h^2(\nu - \nu_i)^2}{2\sigma_i^2}\right\} g_i e^{-\varepsilon_i/T} \quad (3.5.1)$$

Such a method should improve on the PRTA with constant variance σ_K in Eq. (2.3). It has the apparent advantage of involving only K lines compared to N_{est} lines in the R-PRTA scheme ($K \ll N_{est}$, see Tables 1 and 2) to generate the spectrum. On the other hand, the different σ_i implies that the total Gaussian width (combined Doppler plus σ_i) is different for each of the K lines and the efficient FFT method [21] is not applicable. The computational efficiency of the FFT method is demonstrated in Section 4.

4. Stellar envelope opacities

There are several types of variable stars whose pulsations are driven by the κ -mechanism [24]. Originally proposed by Eddington [25], the κ -mechanism works by having an increase in the photon absorption coefficient in some parts of the star at the moment of maximum compression creating the instability. Thus, the study of stellar pulsations provides indirect tests

of opacities and has stimulated research. The “Z bump” is an important example, originally invoked to resolve mass discrepancies [26], soon after predicted by new opacity calculations [27,28], later corroborated by laboratory experiments [29] as well as pulsation studies [30], and now a standard feature in astrophysical opacities [31]. The Z bump is due to photon absorption by iron group elements. Not surprisingly Fe has received considerable attention from theoretical and experimental efforts for over 2 decades [32,33].

At matter conditions relevant to stellar envelopes the transition arrays are complex (partially filled M-shell electronic configurations in Fe) and the spectral lines do not overlap so UTA approaches significantly overestimate the opacity [6]. Furthermore, the spin-orbit interaction is not negligible and intermediate coupling is necessary for DLA calculations [34]. These circumstances have presented a computational challenge for theoretical opacity models.

The numerical example considers the Rosseland and Planck opacities of Fe at temperature and density $T = 20\text{eV}$ and $\rho = 10^{-4}\text{g/cm}^3$. The spectrum is computed on a uniform photon energy mesh with 10^4 points in the range $0 \leq h\nu \leq 20T$. All the calculations use the same initial set of configurations made sufficiently large that additional configurations had negligible impact on the Rosseland opacity. To minimize the effort the configuration term structure is neglected for transition arrays in the energy range $h\nu \leq 0.4T$. These spectral lines are overwhelmed by inverse bremsstrahlung and contribute little to the Rosseland mean average. The intrinsic line profiles include Doppler broadening and a Lorentz-type profile with a frequency dependent collisional width [23]. The calculations are performed with the TOPAZ opacity code [35] with the bound-bound spectrum modified by the models described below in Sections 4.1 through 4.3.

4.1 DLA and UTA models

There are two standard line-by-line calculations: one with intermediate coupling (DLA) and the other with pure LS coupling (DLA-LS). For the present comparisons, the former is considered the best result and used as reference for the other calculations. There is also a calculation using the UTA model [2] (UTA-LS).

4.2 Hybrid PRTA and R-PRTA models

Calculations are done using either the PRTA or the R-PRTA models to complement DLA calculations with intermediate coupling using the following recipe. Firstly, since the primary purpose of the PRTA based models is to improve on the UTA approximation whenever the DLA

method is deemed impractical, transition arrays with a small number of lines are done explicitly with DLA in intermediate coupling; hence, the terminology hybrid PRTA and hybrid R-PRTA. Here the limit is set at $N_{\text{limit}} = 3 \times 10^4$ lines for individual transition arrays.

Secondly, the active subshells are always included in the main group. Furthermore, the maximum number of subshells in the main group is limited by

$$M_K = \text{Min}[M - 2, 4] \quad (4.2.1)$$

where M is the total number of open subshells. For $M_K \geq 3$, the first passive subshell included in the main group is the one with the largest contribution to the variance,

$$\alpha_3(g_3 - \alpha_3)\Omega_{LS}^2(\lambda_3\eta_1 \rightarrow \lambda_3\eta_2) = \text{Max}\left\{\alpha_m(g_m - \alpha_m)\Omega_{LS}^2(\lambda_m\eta_1 \rightarrow \lambda_m\eta_2)\right\}_{m=3}^M \quad (4.2.2)$$

If a fourth subshell is to be included in the main group it is the subshell with the next largest variance. Note that a fourth subshell is included if

$$\frac{\alpha_4(g_4 - \alpha_4)\Omega_{LS}^2(\lambda_4\mu_1 \rightarrow \lambda_4\mu_2)}{\alpha_3(g_3 - \alpha_3)\Omega_{LS}^2(\lambda_3\mu_1 \rightarrow \lambda_3\mu_2)} > 0.1 \quad (4.2.3)$$

and

$$\frac{\sigma_K^2(3 \text{ subshells})}{\sigma_{LS}^2} > 0.3 \quad (4.2.4)$$

otherwise only 3 subshells define the main group. The selection of the main group follows that used in JJ coupling calculations [9].

4.3 Hybrid UTA models

An important application of PRTA models is to make spectrum calculations more efficient without introducing significant uncertainties. It is then fitting to assess the PRTA models described in Section 4.2 by contrasting them with a hybrid scheme that complements the DLA method with the UTA approach. Here the line limit switch from DLA to UTA-LS [2] is set the same as for the hybrid PRTA models.

4.4 Explanation of Table 3

The total number of spectral lines, N_{tot} , in the various calculations are given in Table 3. Rather than giving absolute numbers for the mean opacities, the results are compared to the DLA with intermediate coupling. That is,

$$\bar{\kappa}_{\text{mean}} = \kappa_{\text{mean}}[\text{model}] / \kappa_{\text{mean}}[\text{DLA}] \quad (4.4.1)$$

where $\kappa_{mean}[\text{model}]$ and $\kappa_{mean}[\text{DLA}]$ refer to the mean opacity (Planck or Rosseland) for a given model and DLA with intermediate coupling, respectively.

The total computation times in these calculations are dominated by

$$t_{tot} \approx t_{scf} + t_{atm} + t_{spec} \quad (4.4.2)$$

where t_{scf} , t_{atm} , and t_{spec} respectively refer to the computation time for the self-consistent field and radial integrals, the atomic data (line energies and strengths), and the bound-bound spectrum generation from the spectral lines. Since t_{scf} is identical for all calculations and not relevant to the present discussion, it is excluded in the comparisons. Furthermore, absolute times are not particularly interesting since they depend on computer related details (e.g. processor speed and compiler). Therefore, all reported times are scaled by

$$\text{time unit} = (t_{atm} + t_{spec})[\text{DLA}] \quad (4.4.3)$$

arbitrarily using the DLA calculation with intermediate coupling as reference.

4.5 Discussion of results

The Fe frequency dependent opacity calculations are displayed in Fig. 12 for DLA with intermediate coupling, hybrid R-PRTA, and hybrid UTA. The figure shows good agreement between DLA and hybrid R-PRTA except in regions of weak photon absorption; in particular, the energy range $4T \leq h\nu \leq 6T$. The opacity from the hybrid PRTA model is not shown but it is similar to the hybrid R-PRTA calculation except that the hybrid PRTA has slightly larger discrepancies with the full DLA spectrum in the weak absorption regions. The hybrid UTA spectrum is almost identical to the UTA result (not shown) except for some DLA lines superimposed on the background absorption from arrays computed in the UTA approximation. Clearly, the hybrid UTA model does not reproduce the porosity of the spectrum.

The Rosseland opacity is a harmonic mean that is sensitive to weak photon absorption regions. Table 3 shows that the UTA and pure DLA-LS models respectively overestimate and underestimate the Rosseland opacity in cases where there is no significant line overlap. The hybrid PRTA and hybrid R-PRTA models are in good agreement with the DLA result for the Rosseland mean opacity and are ~ 30 and ~ 20 times faster, respectively. The timesaving in the PRTA based methods results from having about 1/2 of the transition arrays not treated with the full DLA (exceed 3×10^4 line limit).

There is excellent agreement for the Planck opacity in Table 3 except for the UTA models, which have -10% error. Since UTA type models conserve the strength of the transition arrays and the Planck opacity is an arithmetic mean, the disagreement is due to the assumed statistical population of initial levels in the UTA models. Clearly, the PRTA based models, which include Boltzmann weighting of the initial level populations from the small-scale DLA main group calculations, account for most of the spectrum dependence on initial level populations.

The relative computation times in Table 3 show that the extra cost of the R-PRTA over the PRTA is the significant larger number of lines involved in the spectrum generation. Using the efficient FFT method [21], however, the time only increases by ~70%. In contrast, the usual approaches to generate the spectrum depend linearly on the number of lines and would have increased the computation time by over a factor of 70.

The deficit in the number of lines in the DLA versus hybrid R-PRTA calculations in Table 3 is not due to large errors in the estimated number of lines in the latter. It is mostly explained by having some transition arrays in the DLA calculation with intermediate coupling requiring more computer memory than available so these few arrays were computed using pure LS coupling. It means that the reported timesaving relative to the DLA are lower limits since the DLA calculation already contains some compromises.

Finally, the switch in the calculations was set at the relatively low limit $N_{\text{limit}} = 3 \times 10^4$ lines [1]. A more conservative choice, say $N_{\text{limit}} = 10^5$ decreases the error in the Rosseland mean opacity from ~5% to ~2% in the PRTA based calculation with less than ~20% increase in computational effort. On the other hand, an aggressive limit, $N_{\text{limit}} = 10^4$, increases the overestimate of the Rosseland mean opacity to ~20% in the PRTA based calculations without much reduction in computational effort.

5. Conclusions

The partially resolved transition array (PRTA) method developed for JJ coupling [9] was extended to intermediate coupling. The PRTA scheme uses the additive form of the variance formula to split the single feature in the unresolved transition array (UTA) approach into a series of Gaussians while conserving known properties. The method separates the open subshells in the transition into main and secondary groups. The main group is treated with a detail line accounting (DLA) method while the secondary group is treated statistically. The secondary

group contributes to the spectrum by assigning their portion of the variance, which is computed from existing analytic formulas, to each line from the small-scale DLA calculation. By construction the impact of the secondary group on the spectrum is relatively small, but it can dramatically increase the computational effort in the full DLA calculations. Thus, the PRTA method significantly accelerates calculations providing better accuracy than UTA type models.

The PRTA conserves the strength-weighted energy mean and variance of the transition array. It also improves on the higher energy moments and corrects for initial level populations in a systematic manner. An important feature of the PRTA model with intermediate coupling is the accurate reproduction of the progressive transition from a single feature in near-LS conditions towards the spin-orbit split relativistic sub-arrays.

The PRTA approach was also extended to simulate DLA calculations. Such statistical methods require the strength-energy distribution, which is not known and is often approximated by formulas containing free parameters constrained by known exact results [8,16,17]. The proposed random PRTA (R-PRTA) scheme starts with the small-scale DLA calculation for the main group. The model then splits the small-scale DLA lines using a variable line number and variance still conserving the known transition array properties. The procedure approximates the coupling of the main and secondary groups relying on general properties of transition arrays. Only the line splitting produced by the secondary electrons is treated randomly so that initial level population effects are retained. The numerical examples show that the R-PRTA calculations of line spectra are in good agreement with full DLA results. The R-PRTA model provides better fidelity of the DLA results than the PRTA model with only a small overhead in computational effort. In particular, the PRTA scheme does not reproduce the porosity of the spectrum overestimating the photon absorption in between the lines.

The PRTA models were applied to Rosseland mean opacity calculations of Fe at conditions relevant to stellar envelopes. The comparison showed not only good agreement with the DLA calculations for the Rosseland mean opacity but also the frequency dependent photon absorption. It is expected; therefore, that PRTA based method should significantly accelerate opacity calculations without introducing large uncertainties.

Acknowledgments: This work performed under the auspices of the U.S. Department of Energy by Lawrence Livermore National Laboratory under Contract DE-AC52-07NA27344.

Appendix

Conservation of total array variance

Compact formulas are available for the strength-weighted energy mean and variance for the array of lines produced by a dipole radiative transition linking two electronic configurations. [2,3]. The proposed PRTA and R-PRTA models conserves these quantities.

A.1 PRTA model with constant variance

Consistent with Eq. (2.3), the envelope for the line strengths generated by the small-scale DLA component of the PRTA model is given by

$$I_C(\nu) = \frac{h}{S_K \sigma_K \sqrt{2\pi}} \sum_{i=1}^K s_i \exp\left\{-\frac{h^2(\nu - \nu_i)^2}{2\sigma_K^2}\right\} \quad (\text{A.1.1})$$

with normalization

$$\int_{-\infty}^{\infty} d\nu I_C(\nu) = 1 \quad (\text{A.1.2})$$

The sum is over the K lines from the small-scale DLA calculation with total strength

$$S_K = \sum_{i=1}^K s_i \quad (\text{A.1.3})$$

and s_i the strength of the i^{th} line. By construction the PRTA model has

$$S_K^{-1} \sum_{i=1}^K s_i (h\nu_i)^2 + \sigma_K^2 = \sigma_{tot}^2 \quad (\text{A.1.4})$$

where without loss of generality it is assumed that the first moment vanishes (i.e. ν represents the detuning from the mean energy of the K lines).

The variance of $I_C(\nu)$ is given by

$$\begin{aligned} h^2 \int_{-\infty}^{\infty} d\nu \nu^2 I_C(\nu) &= \frac{h^3}{S_K \sigma_K \sqrt{2\pi}} \sum_{i=1}^K s_i \int_{-\infty}^{\infty} d\nu \nu^2 \exp\left\{-\frac{h^2(\nu - \nu_i)^2}{2\sigma_K^2}\right\} \\ &= S_K^{-1} \sum_{i=1}^K s_i (h\nu_i)^2 + \sigma_K^2 = \sigma_{tot}^2 \end{aligned} \quad (\text{A.1.5})$$

Thus, the PRTA model conserves the total transition variance.

A.2 The PRTA model with variable variance

An assumption in the PRTA model [9] is that each of the K lines generated from the small-scale DLA calculation for the main group has identical variance given by the contribution of the

secondary group. It is expected, however, that each of the total angular momentum levels in the main group yield a different variance when coupled to the secondary group, but still conserve the total array variance. A more general expression for the line strength envelope is given by

$$I_V(\nu) = S_K^{-1} \sum_{i=1}^K s_i \frac{h}{\sigma_i \sqrt{2\pi}} \exp\left\{-\frac{h^2(\nu - \nu_i)^2}{2\sigma_i^2}\right\} \quad (\text{A.2.1})$$

where the σ_i need not be the same. The variance for $I_V(\nu)$ should satisfy

$$\begin{aligned} 0 &= \sigma_{tot}^2 - h^2 \int_{-\infty}^{\infty} d\nu \nu^2 I_V(\nu) \\ &= \sigma_K^2 - S_K^{-1} \sum_{i=1}^K s_i \sigma_i^2 \end{aligned} \quad (\text{A.2.2})$$

providing a constraint on the choice for the σ_i 's.

A.3 The R-PRTA model

The R-PRTA model makes the assumption

$$\sigma_i^2 = C \frac{n_i}{s_i} \sigma_K^2 \quad (\text{A.3.1})$$

with the proportionality constant C a free parameter. Substituting Eq. (A.3.1) into the constraint (A.2.2) yields

$$C = S_K / N_{est} \quad (\text{A.3.2})$$

where the results uses the normalization in Eq. (3.1.2) for the estimated total number of lines in the transition array. These results lead to the variable variance σ_i in Eq. (3.1.2).

References

- [1] Q. Porcherot, J. -Ch. Pain, F. Gilleron, T. Blenski, *HEDP* **7**, 234(2011)
- [2] C. Bauche-Arnoult, J. Bauche & M. Klapisch, *Phys.Rev.* **A20**, 2424(1979)
- [3] C. Bauche-Arnoult, J. Bauche & M. Klapisch, *Phys.Rev.* **A31**, 2248(1985)
- [4] F. Gilleron, J. -Ch. Pain, J. Bauche & C. Bauche-Arnoult, *Phys.Rev.* **E77**, 026708(2008)
- [5] J. -Ch. Pain, F. Gilleron, J. Bauche & C. Bauche-Arnoult, *HEDP* **5**, 294(2009)
- [6] C.A. Iglesias & B.G. Wilson, *JQSRT* **52**, 127(1994)
- [7] A. Bar-Shalom, J. Oreg, & W. H. Goldstein, *JQSRT* **51**, 27(1994)
- [8] F. Gilleron, J. Bauche & C. Bauche-Arnoult, *J.Phys. B.* **40**, 3057(2007)
- [9] C.A. Iglesias & V. Sonnad, *HEDP (in press)* <http://dx.doi.org/10.1016/j.hedp.2012.01.001>
- [10] R. Cowan, *The Theory of Atomic Structure* (California Press, Berkeley, 1974)
- [11] J. Bauche, C. Bauche-Arnoult & M. Klapisch, *Advances in Atomic and Molecular Physics*,
Eds. D. Bates & B. Bederson (Academic Press, 1988), Vol. 23, PG 131
- [12] D.A. Liberman, *Phys.Rev.* **B2**, 244(1970)
- [13] K.N. Huang et al., *At. Data Nucl. Data Tables* **18**, 243(1976)
- [14] F.P. Larkin, *J. Phys* **B9**, 37(1976)
- [15] R.P. Feynman, N Metropolis & E. Teller, *Phys.Rev.* **75**, 1561(1949)
- [16] J. Bauche et al, *Phys. Rev.* **A44**, 5707(1991)
- [17] P. Duffy et al, *Phys. Rev.* **A44**, 5715(1991)
- [18] J. Bauche & C. Bauche-Arnoult, *J. Phys.* **B20**, 1659(1987)
- [19] J. Bauche & C. Bauche-Arnoult, *Physica Scripta* **T65**, 99(1996)
- [20] W.H. Press et al, *Numerical Recipes* (Cambridge University Press, 1992)
- [21] V. Sonnad & C.A. Iglesias, *HEDP* **7**, 43(2011)
- [22] C.A. Iglesias, *HEDP* **6**, 318(2010)
- [23] C.A. Iglesias et al, *HEDP* **5**, 97(2009)
- [24] J.P. Cox & T. Giulli, *Principles of Stellar Structure* (Gordon & Breach, New York, 1968)
- [25] A.Gautschy, *Vistas Astron.* **41**, 95(1997)
- [26] N. Simon, *ApJ* **260**, L87(1982)
- [27] C.A. Iglesias, F.J. Rogers & B.G. Wilson, *ApJ* **322**, L45(1987)

- [28] C.A. Iglesias & F.J. Rogers, *ApJ* **371**, L73(1991)
- [29] L.B. DaSilva et al, *Phys.Rev.Lett.* **69**. 438(1992)
- [30] P. Moskalik, JR. Buchler & A. Marom, *ApJ* **385**, 685(1992)
- [31] N.R. Badnell et al, *Mon.Not.Astron.Soc.* **360**, 458(2005); and references therein.
- [32] F.J.D. Serduke et al, *JQSRT* **65**, 527(2000); and references therein.
- [33] D. Gilles et al, *HEDP* **7**, 312(2011); and references therein.
- [34] C.A. Iglesias, F.J. Rogers & B.G. Wilson, *ApJ* **397**, 717(1992)
- [35] C.A. Iglesias et al, *JQSRT* **81**, 227(2003)

TABLE 1
Model comparison for 3p → 3d

	DLA		PRTA			
Example	M^a	N^b	M_K^a	K^b	R	Speedup
Fe⁴⁺	4	2,624,815	2	22,329	0.778	~1000
In²⁷⁺					0.741	
Ba³⁴⁺					0.737	
Tm⁴⁷⁺					0.731	

^a Number of open subshells in the full or small-scale DLA calculation.

^b Number of lines in the full or small-scale DLA calculation.

TABLE 2
Model comparison for 2s → 3p

	DLA		PRTA			
Example	M^a	N^b	M_K^a	K^b	R	Speedup
Fe⁵⁺	5	6,983,165	3	26,903	0.996	~1500
In²⁸⁺					0.979	
Ba³⁵⁺					0.956	

^a Number of open subshells in the full or small-scale DLA calculation.

^b Number of lines in the full or small-scale DLA calculation.

TABLE 3
Fe opacity calculation

Model	$\bar{\kappa}_R$	$\bar{\kappa}_P$	N_{tot}	$t_{atm} + t_{spec}$	t_{atm}	t_{spec}
DLA	1.00	1.00	1.18×10^9	1.00	0.91	0.086
DLA-LS	0.71	1.00	8.43×10^7	0.020	0.018	0.002
UTA-LS	1.42	0.90	1.22×10^4	0.001	<0.0005	0.001
Hybrid UTA	1.42	0.90	8.96×10^5	0.014	0.011	0.003
Hybrid PRTA	1.05	1.00	1.69×10^7	0.030	0.014	0.015
Hybrid R-PRTA	1.06	1.00	1.20×10^9	0.044	0.018	0.026

Figure Captions

Fig. 1 Spectrum calculations for Fe^{4+} with $T = 11\text{eV}$ and $\Gamma = 0.01\text{eV}$: DLA (*gray*), PRTA (*solid*), SOSA (*dot-dash*), and UTA-LS (*dash*).

Fig. 2 Same as Fig. 1 for In^{27+} at $T = 190\text{eV}$.

Fig. 3 Same as Fig. 1 for Ba^{23+} at $T = 250\text{eV}$.

Fig. 4 Same as Fig. 1 for Tm^{47+} at $T = 510\text{eV}$.

Fig. 5 Spectrum calculations for Fe^{5+} with $T = 11\text{eV}$ and $\Gamma = 0.1\text{eV}$: DLA (*gray*), PRTA (*solid*), SOSA (*dot-dash*), and UTA-LS (*dash*).

Fig. 6 Same as Fig. 5 for In^{28+} with $T = 190\text{eV}$.

Fig. 7 Same as Fig. 5 for Ba^{24+} with $T = 250\text{eV}$.

Fig. 8 Spectrum calculations in In^{27+} for initial configuration $[\text{Mg}]3p^5 3d^3 4snp$ with $n = 4, 5, \text{ and } 6$ at $T = 190\text{eV}$: DLA (*black*) and R-PRTA (*red*) with $\Gamma = 0.01\text{eV}$ and PRTA($\sigma_K = 0$) (*blue*) with $\Gamma = 0.1\text{eV}$. The ordinate for $n = 5$ and 6 are shifted for clarity.

Fig. 9 Spectrum calculations for Fe^{4+} at $T = 11\text{eV}$ and $\Gamma = 0.01\text{eV}$: DLA (*gray*) and R-PRTA (*solid*).

Fig. 10 Same as Fig. 9 for Ba^{23+} at $T = 250\text{eV}$.

Fig. 11 Same as Fig. 9 for Tm^{47+} at $T = 510\text{eV}$.

Fig. 12 Fe photon absorption at $T = 20\text{eV}$ and $\rho = 10^{-4}\text{ g/cm}^3$: DLA (*red*), hybrid RPRTA (*black*), and hybrid DLA-UTA (*green*).

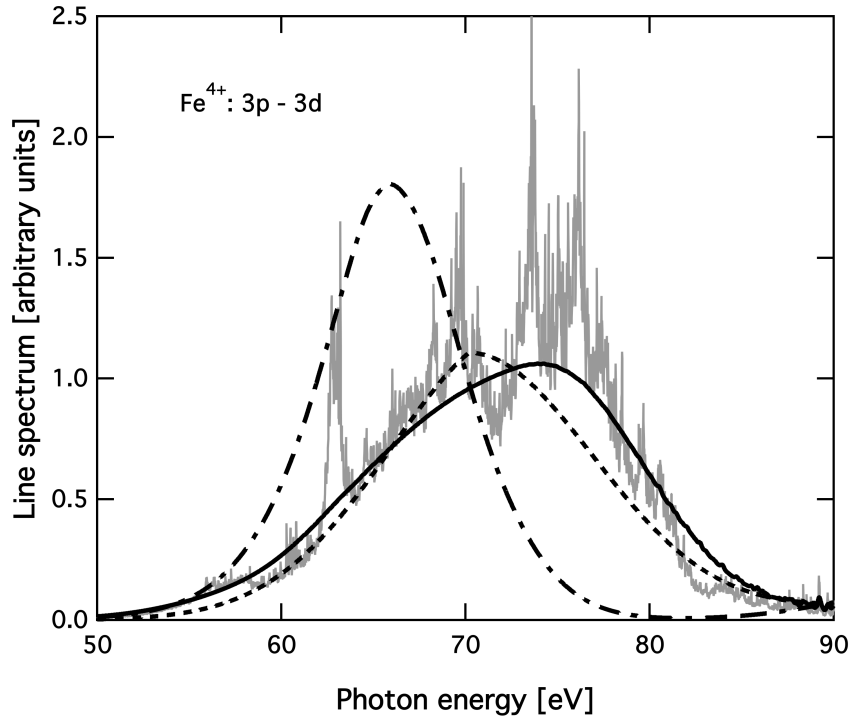


Fig. 1 Spectrum calculations for Fe^{4+} with $T = 11\text{eV}$ and $\Gamma = 0.01\text{eV}$: DLA (*gray*), PRTA (*solid*), SOSA (*dot-dash*), and UTA-LS (*dash*).

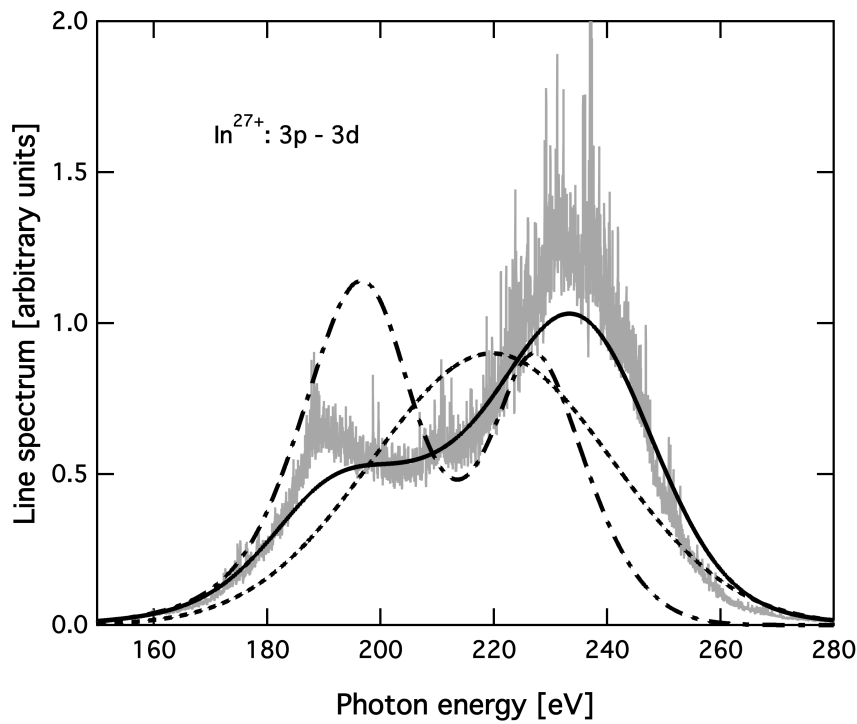


Fig. 2 Same as Fig. 1 for In^{27+} at $T = 190\text{eV}$.

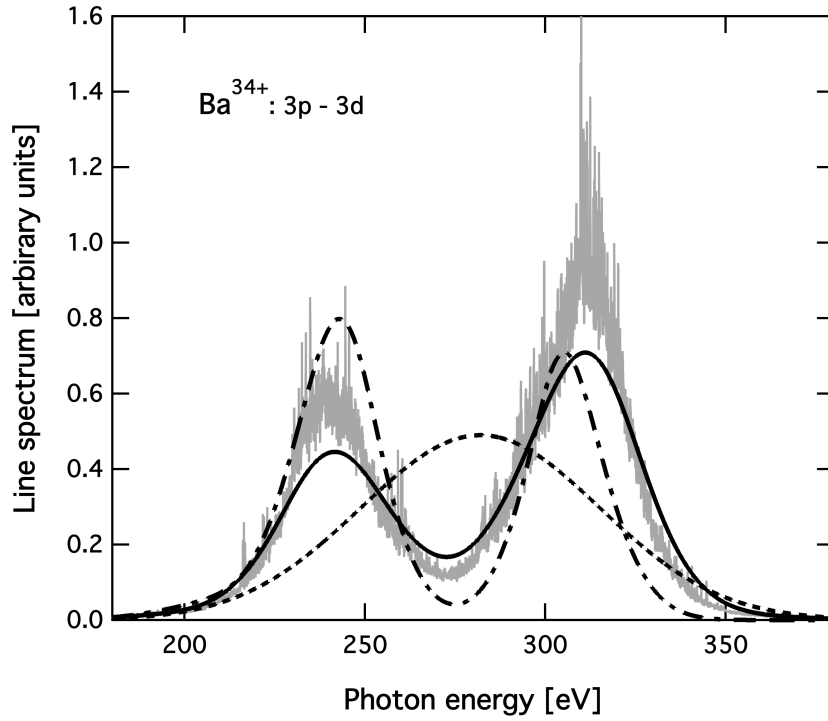


Fig. 3 Same as Fig. 1 for Ba^{23+} at $T = 250\text{eV}$.

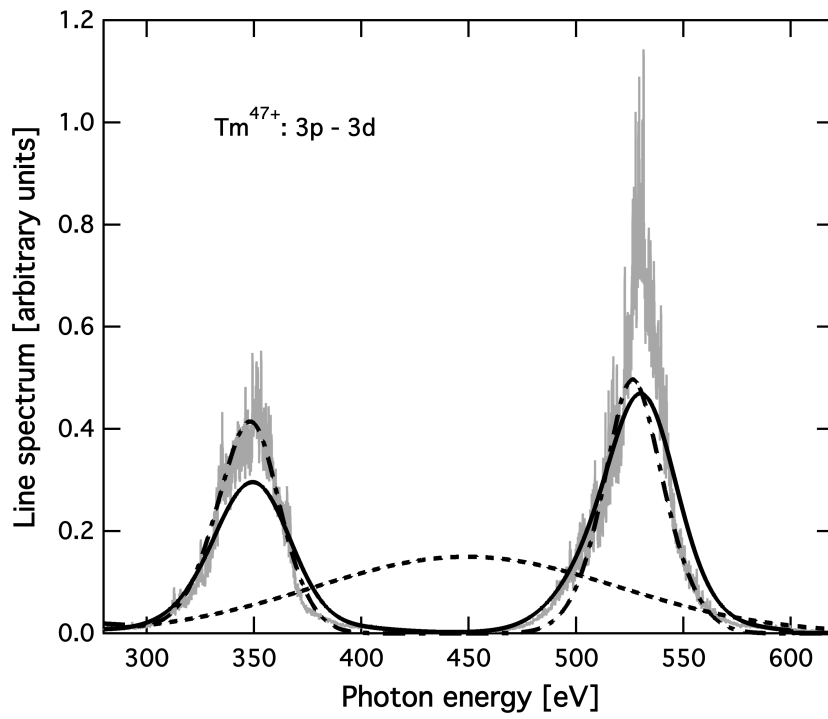


Fig. 4 Same as Fig. 1 for Tm^{47+} at $T = 510\text{eV}$.

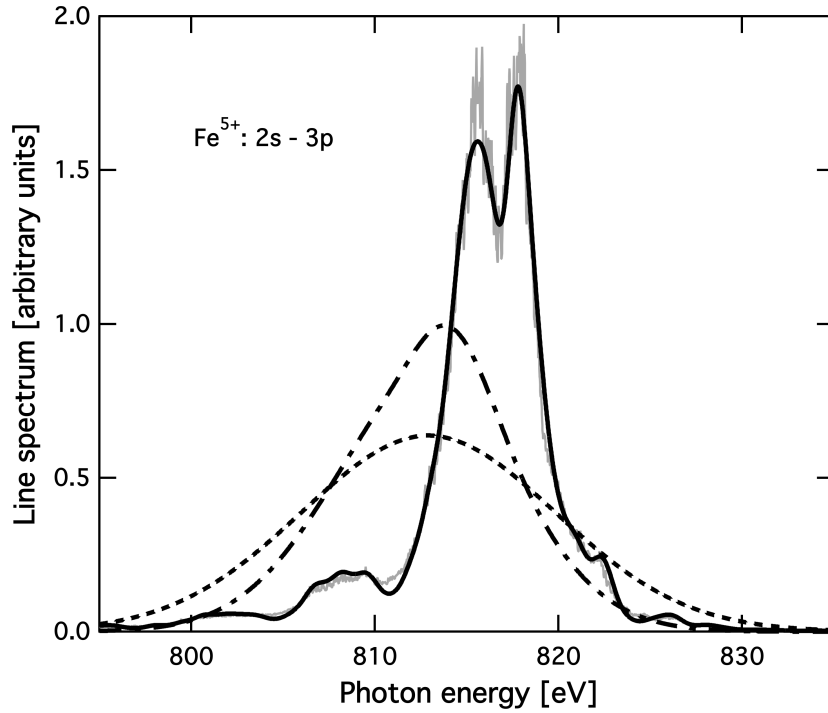


Fig. 5 Spectrum calculations for Fe⁵⁺ with $T = 11\text{eV}$ and $\Gamma = 0.1\text{eV}$: DLA (*gray*), PRTA (*solid*), SOSA (*dot-dash*), and UTA-LS (*dash*).

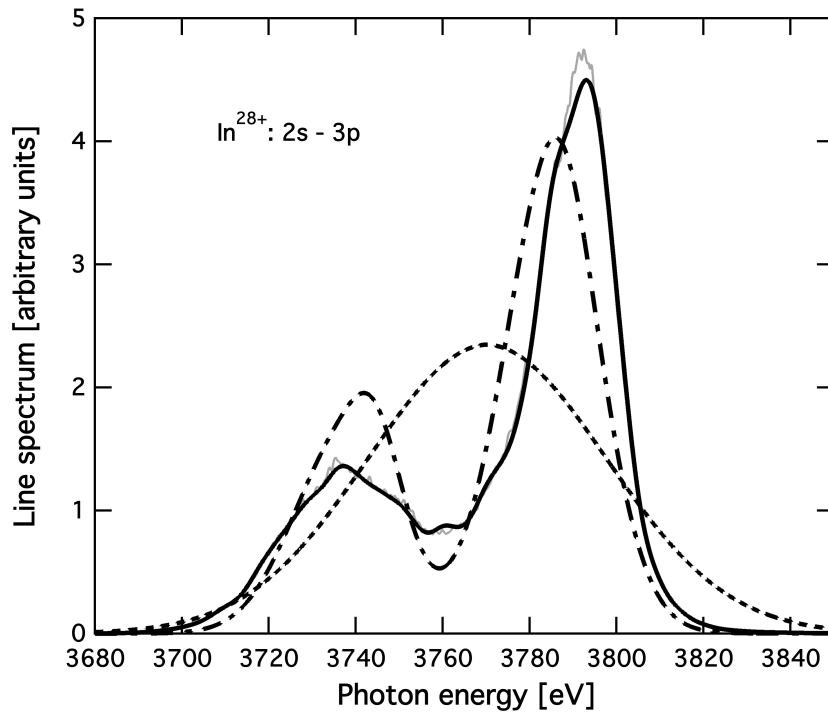


Fig. 6 Same as Fig. 5 for In²⁸⁺ with $T = 190\text{eV}$.

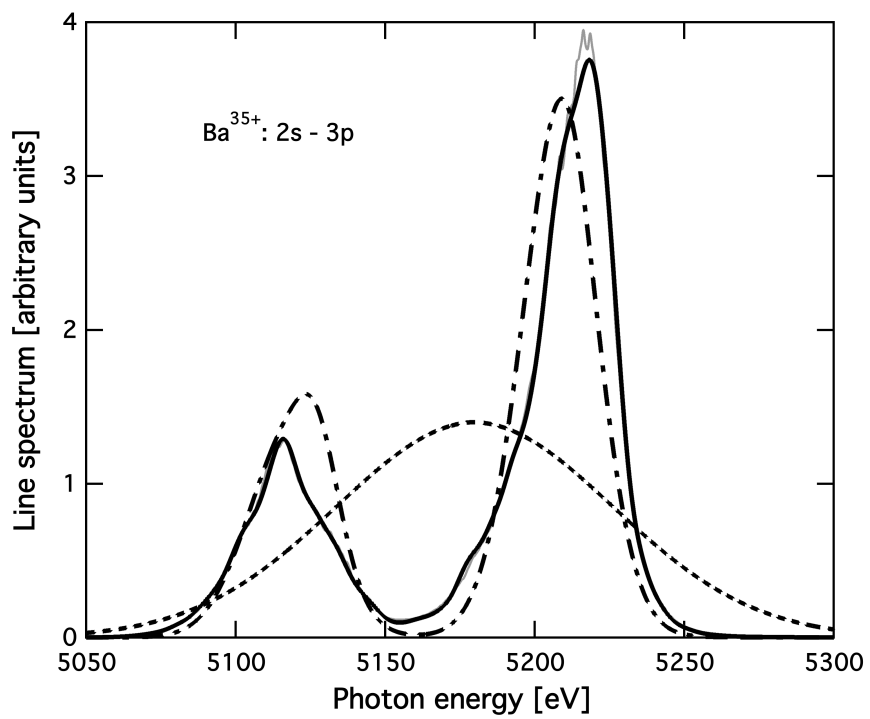


Fig. 7 Same as Fig. 5 for Ba^{24+} with $T = 250eV$.

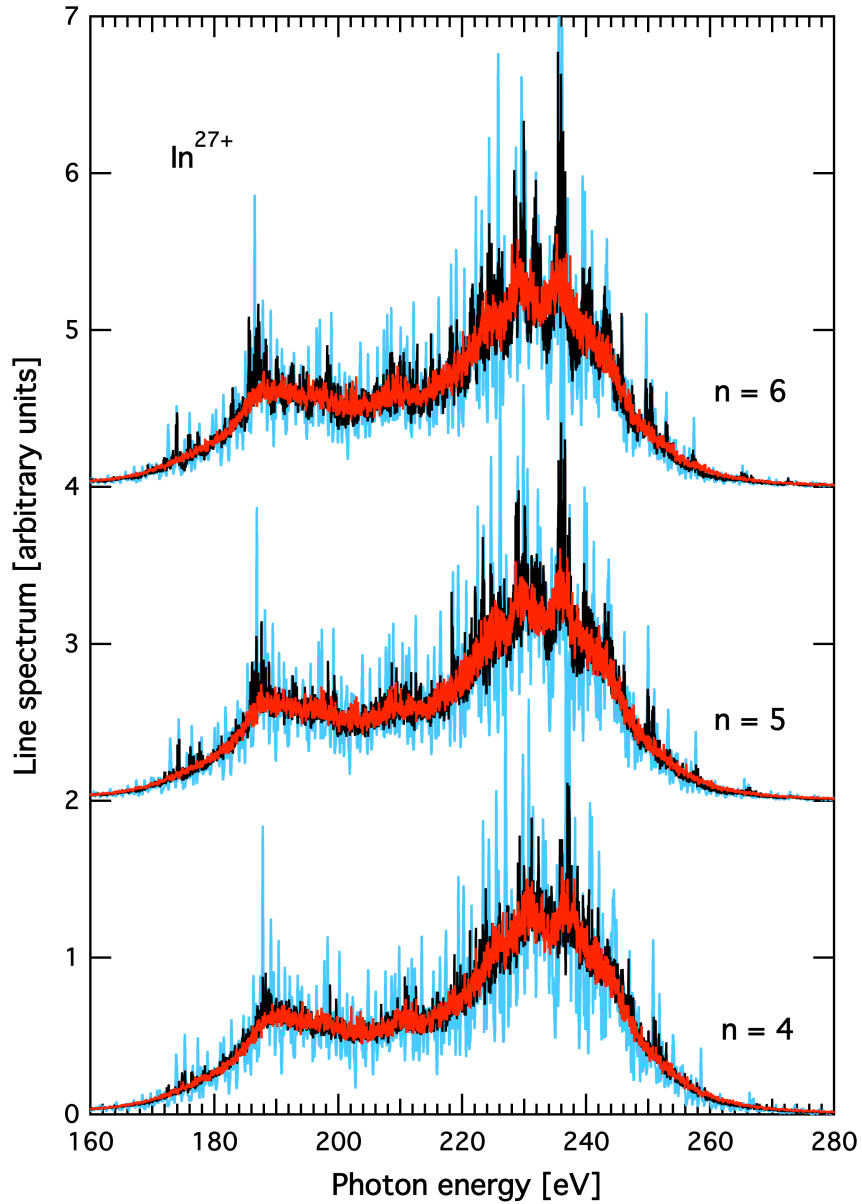


Fig. 8 Spectrum calculations in In^{27+} for initial configuration $[\text{Mg}]3p^5 3d^3 4snp$ with $n = 4, 5$, and 6 at $T = 190\text{eV}$: DLA (*black*) and R-PRTA (*red*) with $\Gamma = 0.01\text{eV}$ and PRTA($\sigma_K = 0$) (*blue*) with $\Gamma = 0.1\text{eV}$. The ordinate for $n = 5$ and 6 are shifted for clarity.

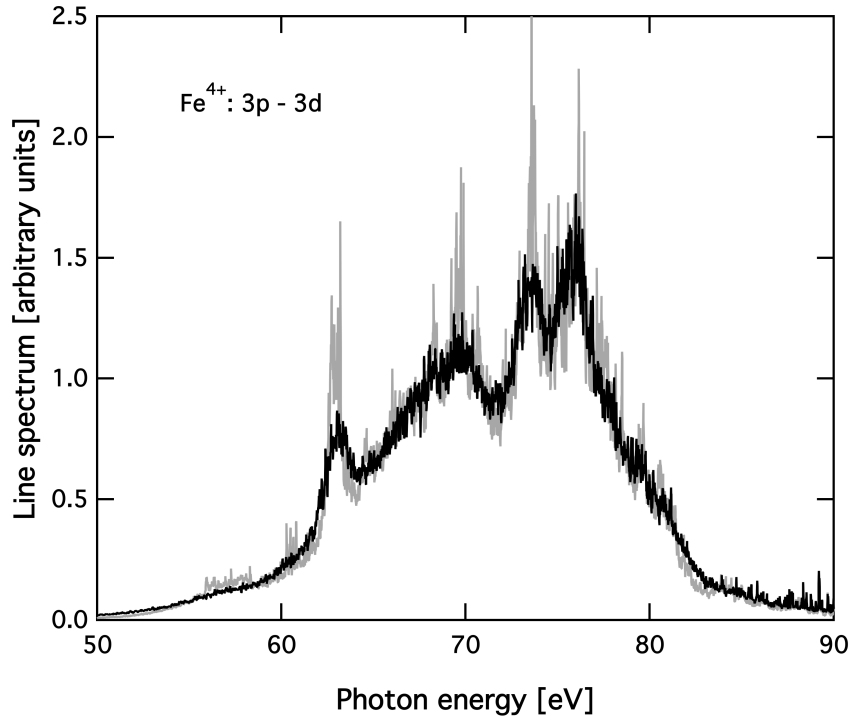


Fig. 9 Spectrum calculations for Fe^{4+} at $T = 11eV$ and $\Gamma = 0.01eV$: DLA (*gray*) and R-PRTA (*black*).

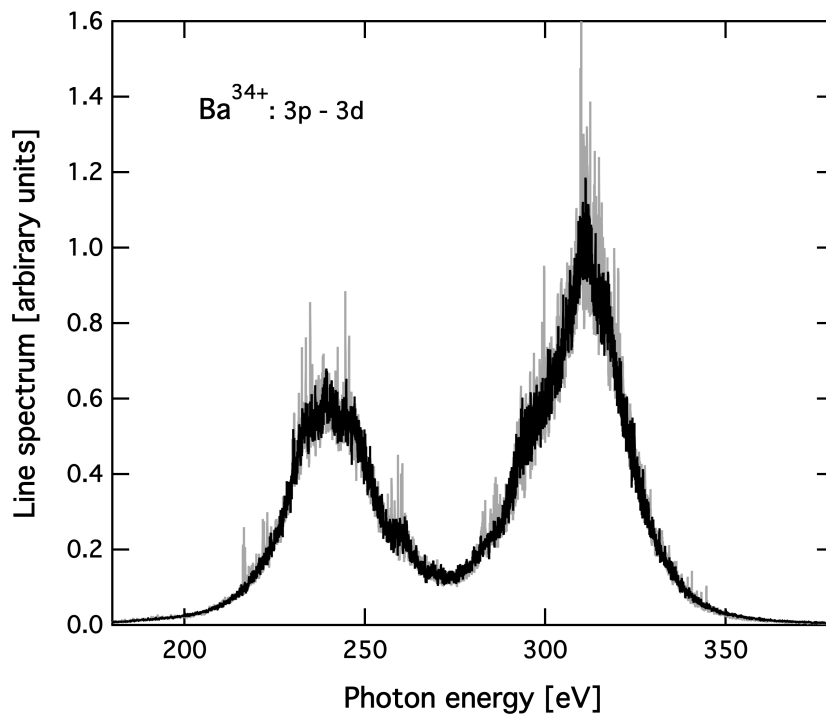


Fig. 10 Same as Fig. 9 for Ba^{23+} at $T = 250eV$.

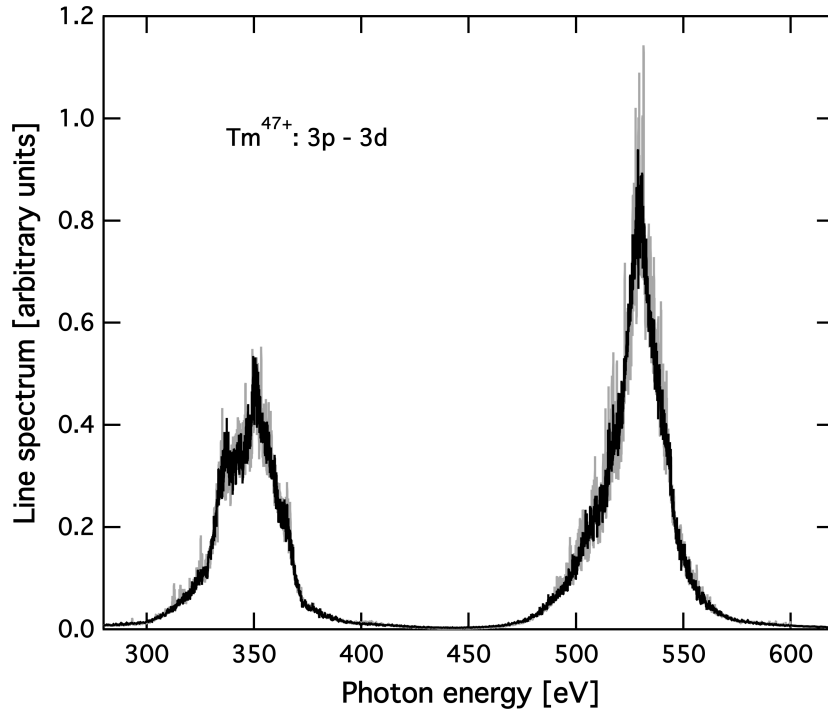


Fig. 11 Same as Fig. 9 for Tm^{47+} at $T = 510\text{eV}$.

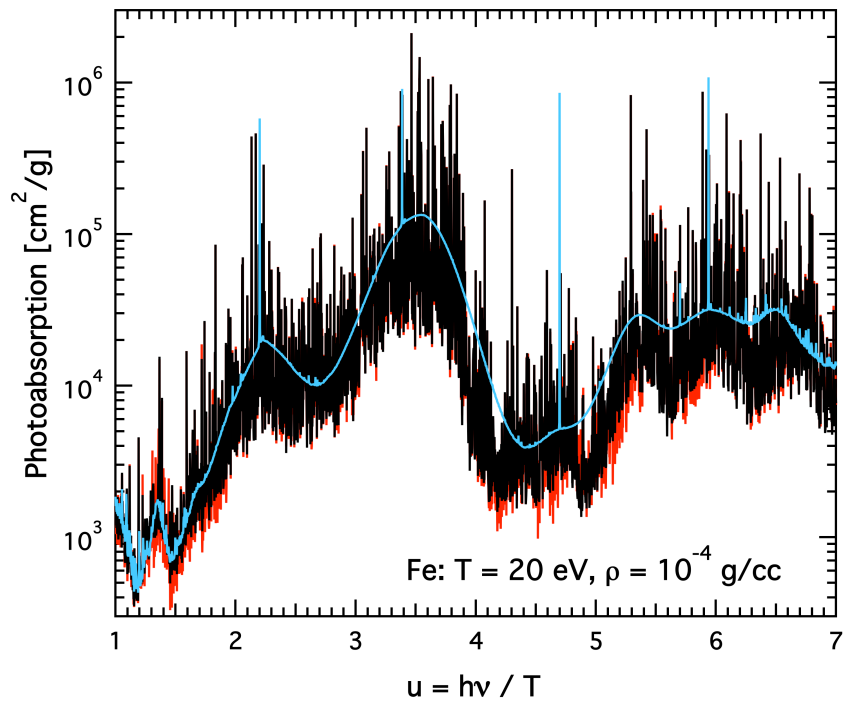


Fig. 12 Fe photon absorption at $T = 20\text{eV}$ and $\rho = 10^{-4}\text{ g/cm}^3$: DLA (red), hybrid RPRTA (black), and hybrid DLA-UTA (green).